Insights into the porous structure of surfactant-promoted gas hydrate

Saphir Venet, Fabrice Guerton, Arnaud Desmedt, Daniel Broseta

▶ **To cite this version:**

Saphir Venet, Fabrice Guerton, Arnaud Desmedt, Daniel Broseta. Insights into the porous structure of surfactant-promoted gas hydrate. Chemical Engineering Science, 2022, 248, pp.117193. 10.1016/j.ces.2021.117193 . hal-03455957

HAL Id: hal-03455957
https://hal.science/hal-03455957

Submitted on 5 Jan 2024

HAL is a multi-disciplinary open access archive for the deposit and dissemination of scientific research documents, whether they are published or not. The documents may come from teaching and research institutions in France or abroad, or from public or private research centers.

L'archive ouverte pluridisciplinaire **HAL**, est destinée au dépôt et à la diffusion de documents scientifiques de niveau recherche, publiés ou non, émanant des établissements d'enseignement et de recherche français ou étrangers, des laboratoires publics ou privés.

Distributed under a Creative Commons Attribution - NonCommercial 4.0 International License

Version of Record: https://www.sciencedirect.com/science/article/pii/S0009250921007582
Manuscript_01921795eafbf0302465230481791da1

Insights into the porous structure of surfactant-promoted gas hydrate

Saphir Venet[a], Fabrice Guerton[a], Arnaud Desmedt[b], Daniel Broseta[a,*]

[a] *Université de Pau et des Pays de l'Adour, E2S UPPA, CNRS, TotalEnergies, LFCR, Pau, France*
[b] *Groupe Spectroscopie Moléculaire, ISM UMR5255 CNRS - Université de Bordeaux, Talence Cedex, France*

Abstract

We show how insights into the porous structure of surfactant-promoted gas hydrate can be obtained from two types of experiments that probe very different length scales. On the one hand, the observation of an existing porous hydrate being imbibed with the aqueous surfactant solution gives information as to the porosity – inferred from the volume increase – and the average pore size – inferred from the imbibition rate. On the other hand, direct pore visualization and determination of the fluid and hydrate contents at the micron scale are obtained by optical microscopy and Raman microspectroscopy. We observe a porosity in the range of 60-70% and pore sizes of about 20-30μm for a porous methane hydrate formed from a 500 ppmw SDS (sodium dodecyl sulfate) solution under moderate subcooling.

Keywords:
methane hydrate, surfactant, sodium dodedyl sulfate (SDS), porous media

Introduction

In quiescent conditions and in the absence of additives, the nucleation and subsequent growth of gas hydrate usually takes place at the interface between the immiscible host (*i.e.*, water) and guest phases, which is rapidly covered with a thin and nearly impermeable polycristalline crust (Beltrán and Servio,

* *Email address:* daniel.broseta@univ-pau.fr (Daniel Broseta)

© 2021 published by Elsevier. This manuscript is made available under the CC BY NC user license
https://creativecommons.org/licenses/by-nc/4.0/

2010; Martínez de Baños et al., 2016; Hassanpouryouzband et al., 2020). Due to the very low transfer rates of water and guest molecules, this crust thickens very slowly, with rates orders of magnitude below lateral growth rates over the water-guest interface, and most of the water and guest molecules on both sides of the interface remains unconverted.

For nearly three decades, the presence of surfactants dissolved in tiny amounts (below the critical micelle concentration) in the water phase has been observed to drastically speed up the conversion into gas hydrate of a quiescent water and guest phases (Kalogerakis et al., 1993; Zhong and Rogers, 2000; Gayet et al., 2005; Watanabe et al., 2005a; Okutani et al., 2008; Karanjkar et al., 2012; Wu et al., 2020). A porous and highly permeable hydrate structure forms, through a process sometimes referred to as capillary-driven. In this process, the aqueous phase is continuously pumped into the growing porous hydrate structure and driven to its border, where it is converted into hydrate. Even though there are exceptions (Karanjkar et al., 2012), anionic surfactants seem to be more effective than non-ionic surfactants (Daniel-David et al., 2015). The guest phase has a strong influence as well, with for instance methane being more prone than CO_2 to capillary-driven hydrate growth (Daniel-David et al., 2015; Dicharry et al., 2016; Molokitina et al., 2019).

This Short Communication reports and exploits two types of experimental observations that provide new insights into the structure of porous methane hydrate grown from a surfactant solution. The first type of experiments monitors the growth of an existing porous hydrate put in contact with the surfactant solution. The second type of experiments determines the hydrate and liquid proportions down to the micron scale. In all experiments, the porous hydrate is formed from methane and pure water containing a low concentration (500 ppmw) of an anionic surfactant, sodium dodecyl sulfate (SDS), under the pressure and temperature of 40 bar and 0°C, which corresponds to a subcooling (or distance to the equilibrium temperature) – slightly above 4°C.

Results

The first type of experiments has already been presented in this Journal (Daniel-David et al., 2015), but not exploited for the features of interest: porosity and pore sizes. Some of the observations are depicted in Figure 1 (see also movie M2 in Daniel-David et al. (2015)). In these experiments, a

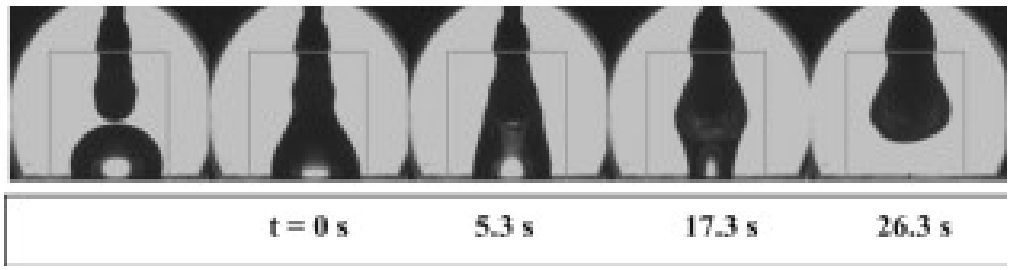

Figure 1: A porous hydrate hanging at the tip of a capillary (with external diameter *ca.* 1.23 mm) is contacted (t=0 s) with a drop of an aqueous surfactant solution sitting on a substrate. This solution rapidly imbibes the porous structure, which expands axisymmetrically and is stabilized within less than 1 minute. From Figure 8 of Daniel-David et al. (2015).

porous methane hydrate formed (shortly before) from a pendant drop of the aqueous surfactant solution and hanging at the tip of a capillary is put in contact with a drop of the surfactant solution sitting on a substrate (two leftmost images in Figure 1) in a closed vessel. This contact triggers a rapid imbibition of the drop into the hanging porous hydrate, which then swells and reaches within a few tens of seconds a novel equilibrium state with a larger volume. Pressure and temperature do not exhibit any detectable change over the duration of the experiment. In fact, the gas (methane) phase occupies a (closed) volume of 17 cm^3, about 2 orders of magnitude that of the drop of liquid water, part of it is transformed into methane hydrate. In addition, the temperature sensor is located far from the hanging drop, where the methane hydrate is formed (Daniel-David et al., 2015). Figure 2 (left) shows the contours of the hanging porous hydrate in its initial state (before contact with the water drop, lefmost image in Figure 1) and final state (not shown in Figure 1). Figure 2 (right) shows the external contours of the porous hydrate plus the underlying aqueous solution ascending into the porous hydrate at various times (from t=0 to 21 s) following contact.

The difference between the final and initial volumes, *ie.*, the volume of the added porous hydrate ΔV, with porosity ϕ, has two contributions: the porous volume $\phi\Delta V$ filled with the SDS solution, and the volume of the hydrate skeleton $(1-\phi)\Delta V$. The volume ΔV is obtained by assuming axisymmetry:

$$\Delta V = \sum_k \pi/4[D_f(k)^2 - D_i(k)^2]v \tag{1}$$

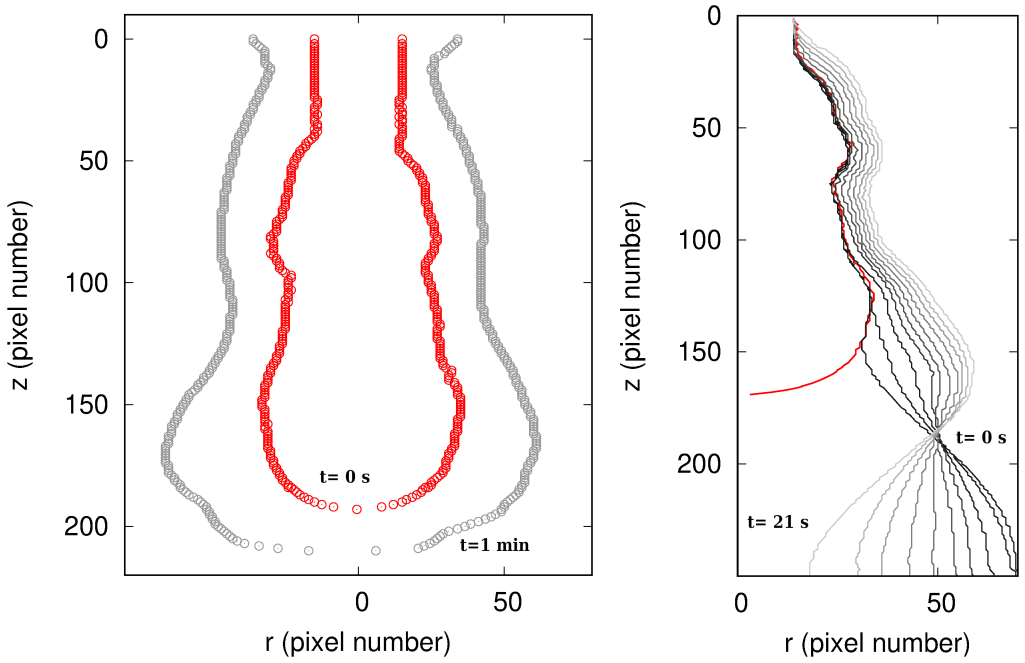

Figure 2: Left: Contours of the initial (t=0 s, in red) and final (t ≈1 minute, in grey) states of the porous hydrate. Right: Contours of the porous hydrate and the liquid water ascending from the water drop at the bottom from t=0 to 21 s. The time interval between two consecutive contours is 2.4 s. The red curve correspond to the initial time (t=0). The scales on the two axis correspond to pixel numbers along the radial and vertical directions.

where $D_f(k)$ and $D_i(k)$ are the horizontal diameters (in number of pixels) of the final (f) and initial (i) porous hydrate at position (or pixel number) k along the vertical direction z, and v is the voxel volume. We obtain ΔV=69.65 mm^3, to be compared with the volume of the water drop, obtained from its contour (data not shown), V_w=64.9 mm^3. The volume expansion, about 5 mm^3, is due to the fact that water molecules occupy a larger volume in the hydrate than in liquid water. Equating the number of moles of water in the liquid drop to that in the added porous hydrate,

$$V_w/v_w = \phi\Delta V/v_w + (1-\phi)\Delta V/v_h \tag{2}$$

with v_w=18 cm^3 the volume of one mole of liquid water and v_h=22.6 cm^3 the volume occupied by one mole of water in the hydrate (Sloan and Koh, 2008), we obtain a porosity $\phi \approx 67\%$.

From the contours at the bottom of the hydrate mass, see Figure 2 (right), we infer a fairly constant pumping rate in the mm^3.s^{-1} range from about t=5 to close to 20 s; for larger t the water drop has been fully pumped and there is no liquid water left on the substrate (see Figure 1). It is tempting here to interpretate the imbibition rate dV/dt, with $V(t)$ the volume of liquid water having imbibed the porous medium at time t, in terms of a Wahsburn-type model (Cai et al., 2021).

$$dV(t)/dt = 0.5\phi S[R\sigma\delta cos(\theta)/(2\tau\mu)]^{1/2}t^{-1/2} \tag{3}$$

where S is the area of the (constant) cross-section in the direction perpendicular to flow, μ is the fluid viscosity ($\sim$ 1 mPa.s) and θ the contact angle, considered here equal to $\theta = 0$ (complete wetting of the hydrate by the aqueous phase). δ is a pore shape factor and τ the tortuosity, whose ratio is for the sake of simplicity considered equal to 1. $\sigma \sim 50$ mN.m^{-1} is the interfacial tension between the aqueous and gas phases (Watanabe et al. (2005b)). Indeed, the time span is too limited for checking the square root time dependence and, in addition, S varies slightly and is approximated here by $\pi d^2/4$, where $d \sim 2$ mm. Using the cited values for the physical parameters, we obtain a pore radius $R \sim 30$ μm.

The corresponding Jurin height $h = 2\sigma/(\Delta\rho g R) \simeq 30$ cm is well below the height of the porous hydrate (inferior to the cm), which justifies the neglect of gravity effects in Eq. (3). ($\Delta\rho \simeq 1000$ kg.m^{-3} is the density difference between the densities of the aqueous phase and methane gas, and $g = 9.81$ m.s^{-2} is the acceleration due to gravity).

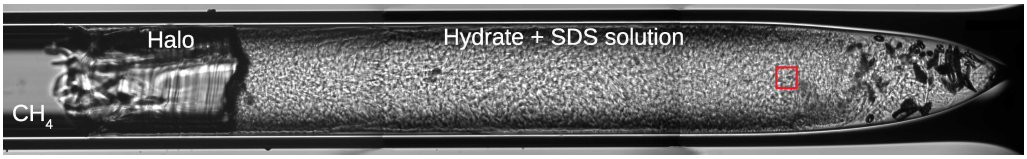

Figure 3: Transmission microscopy image of a porous methane hydrate in a glass capillary of diameter 200 μm. The conversion lasted about 1 hour, starting on the meniscus and propagating to the capillary end on the right. Hydrate methane growth as a halo over the glass capillary wall is apparent near the meniscus. The red square is the region investigated by microRaman spectroscopy, see Figure 4.

The second experiment consists in optical microscopy observations and a characterization by microRaman spectroscopy of the porous hydrate (performed at 532 nm incident wavelenght with a grating of 600 lines/mm and a 50x objective). The spatial resolution is in the μm range, one order of magnitude below that in the first experiment. The optical cell is a thin (internal diameter: 200 μm) glass capillary initially loaded at its sealed end with the surfactant solution, and connected with a high pressure pump filled with methane at 40 bar at its other end, see Atig et al. (2020) for details. Temperature T is controlled by means of a Linkam CAP500 stage and the Linksys software. A hydrate is first formed at very low temperature ($\sim$ -20°C) then immediately melted by rapidly raising T to ($\sim$ 5°C) and then formed again at T equal to 0°C.

The hydrate is continuously generated from the meniscus between the two phases as a flaky structure, which is rejected from the interface into the aqueous solution. About 1 hour later, a homogeneous porous structure replaces the aqueous phase initially present (see Figure 3). The hydrate growth process is slower than that with a drop, because of the very different water/gas interfacial area, limited to the water/gas meniscus in the latter experiment but spanning the whole drop surface in the former. Over this period of time the meniscus advances very slightly to the left, indicating again the highly porous nature of the structure formed. A very thin hydrate halo is observed to grow on the capillary wall on the gas side of the meniscus, riding over a layer of liquid water. This feature is typical of a gas hydrate growing on a water-wet substrate from the triple line formed by the substrate, the aqueous and the guest phases (Beltrán and Servio, 2010; Touil et al., 2017, 2019; Atig et al., 2020).

A Raman microspectroscopy mapping is then performed over a well-

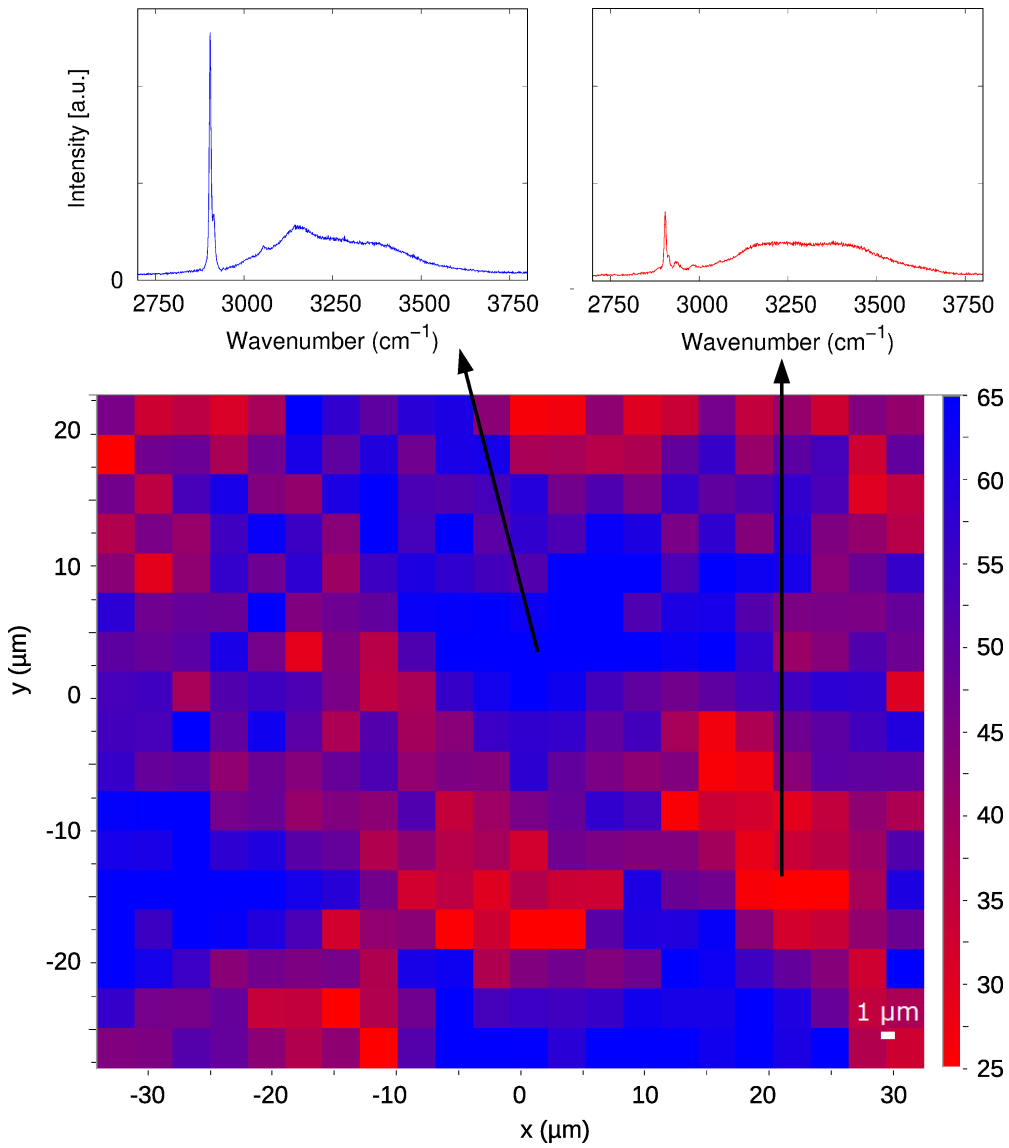

Figure 4: Raman microspectroscopy mapping of the porous methane hydrate formed at 0°C and 40 bar from a 500 ppmw SDS solution. The map has been constructed by considering the methane-to-water Raman band ratio (see text for details). Two types of regions are observed : in blue the areas rich in methane hydrate and in red the areas with a large quantity of liquid water. Acquisition time $\simeq$ 3 hours.

defined cross-section, see Figure 3. The mapping corresponds to spectra acquired in a horizontal plane with dimension 70 μm x 50 μm (the longest distance is along the capillary axis) with a pixel size of 3 μm x 3 μm; for each one of these squares there is one Raman spectrum acquired for wavenumbers in the interval 2700-3800 cm^{-1}, see Figure 4. The broad bands between 3000-3600 cm^{-1} correspond to the water signature, while the narrow band observed at 2905-2915 cm^{-1} corresponds to the stretching modes of the methane confined in the hydrate structure (Sum et al., 1997; Botimer et al., 2015; Chazallon et al., 2017). The Raman mapping has been constructed by considering the intensity ratio of the methane narrow band to the water broad band. Two typical spectra are shown in Figure 4: the blue one with a large methane-to-water intensity ratio corresponds to a hydrate-rich region, whereas the red one with a small methane-to-water intensity ratio is typical of a water-rich region. The water profiles are different in these two typical regions. While the water profile is typical of a hydrate structure in the hydrate-rich region, it is typical of liquid water in the water-rich region, dominating the hydrate water signal (Chazallon et al., 2017).

Clearly, the hydrate formed is porous with a hydrate skeleton and channels filled with liquid water. A porosity is found in the range of 60-80%, dependent on the segmentation procedure. The pores or water-rich domains have sizes in the range of 20-30 μm. These values do not depend on where the Raman mapping has been carried out, whether close or far from the meniscus (data not shown).

Recent experiments carried out under similar SDS concentration and subcooling conditions but in cylindrical vessels much larger than ours (Botimer et al., 2015) revealed a rapid "consumption" of water, as witnessed by a rapid drop of the surface of the aqueous (bulk) solution in the vessel and the formed methane hydrate climbing on the walls. In addition, the uptake of methane was observed to lag water consumption, which the authors (Botimer et al., 2015) attributed to water forming an "intermediate immobile solid-like state" before enclathrating the methane molecules. Our results show that this lag might be explained as follows. At first, only a fraction of the water is converted into the methane hydrate that forms a porous skeleton, while the other fraction remains liquid and occupies the porosity. The latter fraction possibly undergoes a slow conversion into hydrate, which could be addressed in a time-resolved Raman microspectrocopy investigation (left for future work: priority has been given here to spatial resolution).

Even though the two methods presented above provide access to very dif-

ferent length scales, consistent features (porosity and pore size) are found for the structure of the porous hydrate that forms when a surfactant is present in the aqueous phase. They are very promising tools for characterizing and understanding how subcooling and the nature and concentration of the surfactant as well as other additives (nanoparticules, porous media, thermodynamic promoters, etc.)(Liu et al., 2018; Zhang et al., 2020, 2021) could be combined to overcome the mass-transfer bottleneck.

References

Atig, D., Broseta, D., Pereira, J., Brown, R., 2020. Contactless probing of polycrystalline methane hydrate at pore scale suggests weaker tensile properties than thought. Nature Comm. 11, 3379. doi:10.1038/s41467-020-16628-4.

Martínez de Baños, M.L., Hobeika, N., Bouriat, P., Broseta, D., Enciso, E., Clément, F., Brown, R., 2016. How do gas hydrates spread on a substrate? Cryst. Growth Des. 16, 4360–4373. URL: https://doi.org/10.1021/acs.cgd.6b00471, doi:10.1021/acs.cgd.6b00471.

Beltrán, J.G., Servio, P., 2010. Morphological investigations of methane-hydrate films formed on a glass surface. Cryst. Growth Des. 10, 4339–4347. doi:10.1021/cg1003098.

Botimer, J., Dunn-Rankin, D., Taborek, P., 2015. Evidence for immobile transitional state of water in methane clathrate hydrates grown from surfactant solutions. Chemical Engineering Science 142. doi:10.1016/j.ces.2015.11.035.

Cai, J., Jin, T., Kou, J., Zou, S., Xiao, J., Meng, Q., 2021. Lucas–washburn equation-based modeling of capillary-driven flow in porous systems. Langmuir 37, 1623–1636. URL: https://doi.org/10.1021/acs.langmuir.0c03134, doi:10.1021/acs.langmuir.0c03134. pMID: 33512167.

Chazallon, B., Noble, J.A., Desmedt, A., 2017. Spectroscopy of Gas Hydrates: From Fundamental Aspects to Chemical Engineering, Geophysical and Astrophysical Applications. John Wiley & Sons, Ltd. chapter 2. pp. 63–112. URL: https://onlinelibrary.wiley.com/doi/abs/10.1002/9781119332688.

ch2, doi:https://doi.org/10.1002/9781119332688.ch2, arXiv:https://onlinelibrary.wiley.com/doi/pdf/10.1002/9781119332688.ch2.

Daniel-David, D., Guerton, F., Dicharry, C., Torré, J.P., Broseta, D., 2015. Hydrate growth at the interface between water and pure or mixed co2/ch4 gases: Influence of pressure, temperature, gas composition and water-soluble surfactants. Chemical Engineering Science 132, 118 – 127. doi:https://doi.org/10.1016/j.ces.2015.04.015.

Dicharry, C., Diaz, J., Torré, J.P., Ricaurte, M., 2016. Influence of the carbon chain length of a sulfate-based surfactant on the formation of co2, ch4 and co2-ch4 gas hydrates. Chemical Engineering Science 152. doi:10.1016/j.ces.2016.06.034.

Gayet, P., Dicharry, C., Marion, G., Graciaa, A., Lachaise, J., Nesterov, A., 2005. Experimental determination of methane hydrate dissociation curve up to 55 mpa by using a small amount of surfactant as hydrate promoter. Chemical Engineering Science 60, 5751–5758. doi:10.1016/j.ces.2005.04.069.

Hassanpouryouzband, A., Joonaki, E., Vasheghani Farahani, M., Takeya, S., Ruppel, C., Yang, J., English, N.J., Schicks, J.M., Edlmann, K., Mehrabian, H., Aman, Z.M., Tohidi, B., 2020. Gas hydrates in sustainable chemistry. Chem. Soc. Rev. 49, 5225–5309. doi:10.1039/C8CS00989A.

Kalogerakis, N., Jamaluddin, A., Dholabhai, P., Bishnoi, P., 1993. Effect of surfactants on hydrate formation kinetics. doi:10.2118/25188-MS.

Karanjkar, P., Lee, J., Morris, J., 2012. Surfactant effects on hydrate crystallization at the water-oil interface: Hollow-conical crystals. Crystal Growth & Design 12, 3817–3824. doi:10.1021/cg300255g.

Liu, Z., Pan, Z., Zhang, Z., Liu, P., Shang, L., Li, B., 2018. Effect of porous media and sodium dodecyl sulphate complex system on methane hydrate formation. Energy & Fuels 32, 5736–5749. doi:10.1021/acs.energyfuels.8b00041.

Molokitina, N., Nesterov, A., Podenko, L., Reshetnikov, A., 2019. Carbon dioxide hydrate formation with sds: Further insights into mechanism of gas hydrate growth in the presence of surfactant. Fuel 235, 1400–1411. doi:10.1016/j.fuel.2018.08.126.

Okutani, K., Kuwabara, Y., Mori, Y.H., 2008. Surfactant effects on hydrate formation in an unstirred gas/liquid system: An experimental study using methane and sodium alkyl sulfates. Chemical Engineering Science 63, 183–194. doi:https://doi.org/10.1016/j.ces.2007.09.012.

Sloan, E.D., Koh, C.A., 2008. Clathrate Hydrates of Natural Gases. volume 119 of *Chemical Industries*. 3rd ed., CRC Press, Boca Raton, FL.

Sum, A.K., Burruss, R.C., Sloan, E.D., 1997. Measurement of clathrate hydrates via raman spectroscopy. The Journal of Physical Chemistry B 101, 7371–7377. doi:10.1021/jp970768e.

Touil, A., Broseta, D., Desmedt, A., 2019. Gas hydrate crystallization in thin glass capillaries: Roles of supercooling and wettability. Langmuir 35, 12569–12581. URL: https://doi.org/10.1021/acs.langmuir.9b01146, doi:10.1021/acs.langmuir.9b01146.

Touil, A., Broseta, D., Hobeika, N., Brown, R., 2017. Roles of wettability and supercooling in the spreading of cyclopentane hydrate over a substrate. Langmuir 33, 10965–10977. URL: https://doi.org/10.1021/acs.langmuir.7b02121, doi:10.1021/acs.langmuir.7b02121.

Watanabe, K., Imai, S., Mori, Y., 2005a. Surfactant effects on hydrate formation in an unstirred gas/liquid system: An experimental study using hfc-32 and sodium dodecyl sulfate. Chemical Engineering Science 60, 4846–4857. doi:10.1016/j.ces.2005.03.043.

Watanabe, K., Niwa, S., Mori, Y.H., 2005b. Surface tensions of aqueous solutions of sodium alkyl sulfates in contact with methane under hydrate-forming conditions. Journal of Chemical & Engineering Data 50, 1672–1676. doi:10.1021/je050139v.

Wu, Y., Liyan, S., Zhou, L., Zhang, Z., 2020. Progress in use of surfactant in nearly static conditions in natural gas hydrate formation. Frontiers in Energy 14. doi:10.1007/s11708-020-0675-2.

Zhang, G., Zhang, R., Wang, F., 2021. Fast formation kinetics of methane hydrates loaded by silver nanoparticle coated activated carbon (ag-np@ac). Chemical Engineering Journal 417, 129206. URL: https://www.sciencedirect.com/science/article/

pii/S138589472100797X, doi:https://doi.org/10.1016/j.cej.2021.129206.

Zhang, Z., Liu, Z., Pan, Z., Baena-Moreno, F.M., Soltanian, M.R., 2020. Effect of porous media and its distribution on methane hydrate formation in the presence of surfactant. Applied Energy 261, 114373. doi:https://doi.org/10.1016/j.apenergy.2019.114373.

Zhong, Y., Rogers, R., 2000. Surfactant effects on gas hydrate formation. Chemical Engineering Science 55, 4175–4187. doi:https://doi.org/10.1016/S0009-2509(00)00072-5.